ELSEVIER

International Journal of Heat and Fluid Flow 23 (2002) 278–287

International Journal of HEAT AND FLUID FLOW

www.elsevier.com/locate/ijhff

Multi-scale computational heat transfer with moving solidification boundaries ☆

Wei Shyy *

Department of Aerospace Engineering, Mechanics and Engineering Science, University of Florida, 231 Aerospace Building, P.O. Box 116250, Gainesville, FL 32611-6250, USA

Abstract

In order to develop computational strategies for solidification processing of advanced engineering materials, one must address several fundamental issues, including (i) a moving solid–fluid interface, (ii) geometrical complexities of both processing components and solid–fluid interfaces, and (iii) disparate scales in length and time, ranging from the dimension of the processing system, to the convection and diffusion scales, to the morphological scale, and to the capillary scale. Main implications from these observations are that dynamic similarity can not be maintained in virtually any scale-up processes, and, even for laminar flows, direct numerical simulation of a solidification problem can not be handled with current computing resources. In this article, we highlight recent efforts in developing suitable computational techniques to facilitate a multi-scale approach which handles micro-, meso-, and macro-scale phenomena in a coupled framework. Relevant modeling and computational techniques are summarized along with selected examples at macroscopic and morphological scales. © 2002 Published by Elsevier Science Inc.

1. Introduction

The large scale production of high quality crystals and alloys involves a number of complex physical mechanisms typical of solidification processes. These include heat and mass transport, dynamics of moving interfaces, geometrical configurations, material thermo-physical properties, and, most critically, non-linear coupling among them. These complications have traditionally resulted in simplified analyses carried out under quite restrictive assumptions such as idealized geometry, assumed boundary conditions, and constant thermo-physical properties; in these reduced models, important convection modes created by buoyancy and capillary effects, critical in many solidification processes, are also often neglected. Accordingly, the predictive capability of such simplified model is quite limited. A comprehensive macroscopic solidification processing model has to account for geometrical complexities, temperature and phase dependent material properties, buoyancy driven convection and its influence on the melt/crystal interface and the resulting thermal distribution within the crystal. In particular, process scale-up from small laboratory experiments to large production is not well addressed in theory. To accurately simulate the microscopic (morphological) characteristics, information from the macroscopic level needs to be accounted for in much finer length scales in order to address the interaction between thermal and capillary aspects, and their impact on solidified structures. Computational tools can be very valuable for helping us gain physical insight and, based on this insight, improve and optimize the process design. They offer a framework for a convenient and relatively inexpensive platform for performing parametric studies to cover the entire range of processing conditions.

One issue intrinsic to the solidification process is the presence and interaction of different length and time scales in the system. To illustrate this point, let us consider three-dimensionless parameters encountered during many practically important solidification processes, namely, Rayleigh number (*Ra*), Marangoni number (*Ma*), and Stefan number (*St*). A straightforward inspection reveals that these dimensionless parameters scale differently with respect to the geometrical dimensions of the solidification component (*l*): *Ra* is

☆ This paper is a revised and expanded version of a paper presented at CHT'01, the Second International Symposium on Advances in Computational Heat Transfer (Palm Cove, Qld., Australia, 20–25 May 2001), the proceedings of which were published by Begell House, Inc.

* Tel.: +1-352-392-0961, fax: +1-352-392-7303.
E-mail address: wei-shyy@ufl.edu (W. Shyy).

0142-727X/02/$ - see front matter © 2002 Published by Elsevier Science Inc.
PII: S0142-727X(02)00175-3

proportional to l^3, Ma to l, while St is independent of l. Hence, in practical terms, it is impossible to conduct a laboratory experiment that can maintain the same values of all the dimensionless parameters since a change of length scale of the melt impacts different dimensionless parameters differently. In other words, between laboratory and production scales, the relative dominance of different transport mechanisms, such as molecular diffusion, and buoyancy and surface tension driven convection, changes (Shyy, 1994). Furthermore, the Prandtl number and Schmidt number should also be kept unchanged if one wants to study the transport characteristics in a given processing condition, thus substantially restricting one's flexibility of choosing a substitute material which is easier to handle in a laboratory set-up. Experimentally, it is very difficult to maintain a strict similarity of the transport processes between solidification facilities of different length scales via the change of, say, temperature and transport properties to accommodate the variation in l.

In addition to the scaling issue, fundamentally, the presence of multiple scales in time and length makes numerical simulation of solidification dynamics a challenging task. In casting components, the global length scales typically are $l = \mathrm{O}(10^0)$ m. As summarized by Shyy and Udaykumar (2000), for slow growth, with typical values for metals in directional solidification, the diffusion of solute takes place typically at a length scale of $\delta_c = \mathrm{O}(10^{-3})$ m. Interfacial energy typically presents a length scale of $d_0 = \sigma/L$, where σ is the interfacial energy and L is the latent heat of fusion. Typically this gives a scale of $\mathrm{O}(10^{-8}$–$10^{-9})$ m. The resultant microstructural length scale measured by the dendrite tip radius is around $\mathrm{O}(10^{-6})$ m. As an illustration, consider a schematic of the solidification process of a material as shown in Fig. 1. When solidification ensues from the melt the interface between the solid and liquid is seldom planar. Macroscopic undulations of the interface are unavoidable due to the effects of convection. Convection may result due to thermal/solutal buoyancy effects, or

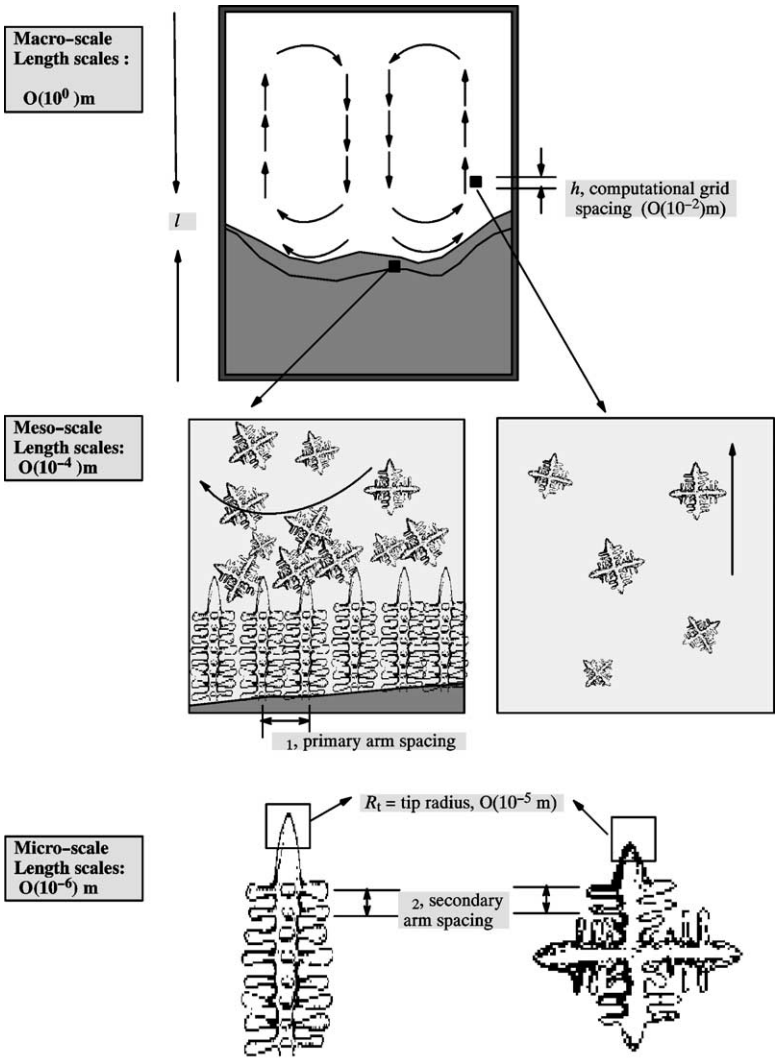

Fig. 1. Illustration of the features and corresponding length scales occurring in the solidification process at the macro-, meso-, and microscales.

surface tension effects, or due to imposed stirring/pouring action. Thus, this global convection pattern gives rise to compositional non-uniformity in the solidified product. Furthermore, in the solidification of alloys, the transition from liquid to solid usually occurs through a two-phase (solid–liquid) layer known as the mushy zone (Flemings, 1974; Shyy, 1994; Worster, 1997). The mushy zone consists of a network of microscopic solid structures which leads to a porous medium-like appearance of this zone. The macroscopic distribution of the solute rejected through the mushy region at the macro-level ("macrosegregation") depends heavily on the characteristics of the mush region.

The importance of the microstructural features for the materials engineer are considerable. These structures present a second level of inhomogeneities in the cast structure, particularly in the form of solutal inhomogeneity due to the rejection of solute from the solid into the liquid and its accumulation in the regions between the solid network. This leads to the "microsegregation" of solute in the final product, and the final grain structure of the solid is determined by these instabilities at the solid–liquid interface. Typical cast structures feature a mixture of grain sizes, orientations and types (columnar/equiaxed) (Flemings, 1974; Hurle, 1993), and prediction/control of the grain structure hinges on controlling the global thermal and convective phenomena in the casting operation so that this desired microstructure can be induced. Thus, there is an intimate connection between the macro-phenomena (at the scale of the casting) and the microstructure obtained.

The split in scales between the macro- and micro-events in the solidification process renders the modeling and computation of industrial casting processes rather difficult. In a simulation it is impossible at present to calculate the processes at all scales at the same time. This situation is akin in some respects to that in modeling of turbulent flows, where direct numerical simulation of all scales is only possible currently for a limited range of flow conditions. For instance, the sensitivity of predicted macro-phenomena to micro-models and to numerical accuracy and resolution has not been addressed. This is even more striking because a large number of the micro-model components are usually modeled by means of augmented dissipation effects (akin to eddy viscosity approaches in turbulence modeling). Furthermore, as pointed out by Shyy et al. (1997), such closure issues exist because of the averaging practice adopted at the theoretical level to account for the effect of unresolvable scales, and the need for subgrid models exists for both laminar and turbulent flows alike. However, in solidification modeling proposed in the literature, these augmented dissipation coefficients are chosen in ad hoc fashion. Therefore, it is difficult to separate physics from the effects of dissipation, both numerical as well as modeled.

In this article, we review some of our recent efforts in developing suitable computational techniques to facilitate a multi-scale approach which handles micro-, meso-, and macro-scale phenomena directly, employing volume averaging as the matching procedure between different scales. The goal is to extrapolate a given materials processing technique from a small size laboratory set-up to a large production size, and to investigate the solidification characteristics at both macroscopic and morphological scales.

2. Multi-scale volume averaging

Various averaging procedures have been proposed, as reviewed by Beckermann and Viskanta (1993) and by Shyy et al. (1997). In addition to the single scale averaging process, Wang and Beckermann (1994, 1996) have presented a dual-scale volume averaging operation. The macro-transport equations are solved at the scale l, shown in Fig. 1. The domain is discretized into a grid of size h. The dual-scale averaging is then required since the micro-transport equations are composed of two predominant scales. These are the processes occurring at the scale involving the grain envelopes (the mesoscale of λ_1, the primary dendrite spacing) and that within each grain which may be characterized by the secondary dendrite arm spacing (the microscale of λ_2). Thus, one first averages over the secondary side branches to obtain the information over the level of a grain. Then one averages the phenomena involving the individual grains to get the behavior at the macro-scale (at scale h). This telescopes the phenomena at two-levels (λ_1 and λ_2) into subgrid scale information at scale h. This implies filtering of information at the resolution λ_2 followed by another filtering at resolution λ_1. The process can be illustrated schematically as in Fig. 2. For any variable ψ, such as the solid fraction f_s, the volume averaging obtains the subgrid representation to be adopted in the macro-scale computations. It is based on the view that such a dual-scale averaging process will provide a better subgrid-scale modeling capability than a single-scale averaging procedure described in Beckermann and Viskanta (1993) and Ganesan and Poirier (1990).

Detailed derivation and associated modeling issues of the single- and dual-scale averaging procedures can be found in Shyy et al. (1997) and Shyy and Udaykumar (2000), respectively. The modeling concept and the relationships between phenomena at the macro-, micro- and mesoscales pertaining to the transport and growth of dendrites in a melt are given in Fig. 3. The approach taken by Shyy and Udaykumar (2000) is to numerically simulate phenomena at each scale by including all the necessary physics such as convection effects, anisotropy and capillarity, differences in material properties, particularly species diffusion coefficients between solid and

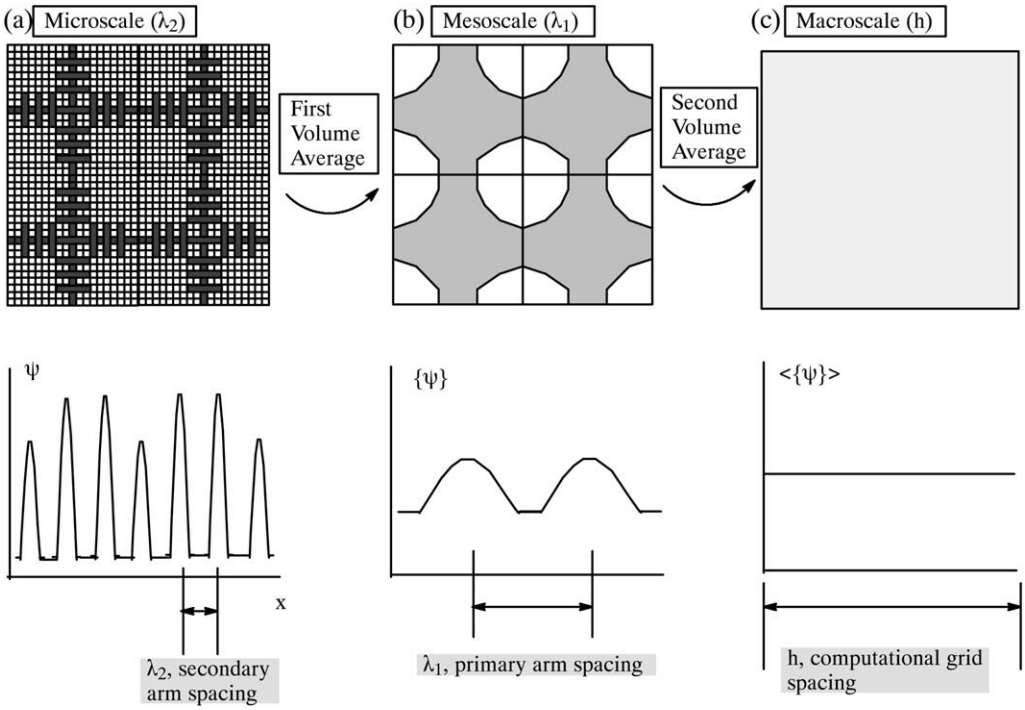

Fig. 2. Illustration of the filtering or averaging process involved in the dual-scale averaging to obtain macroscopic volume-averaged equations.

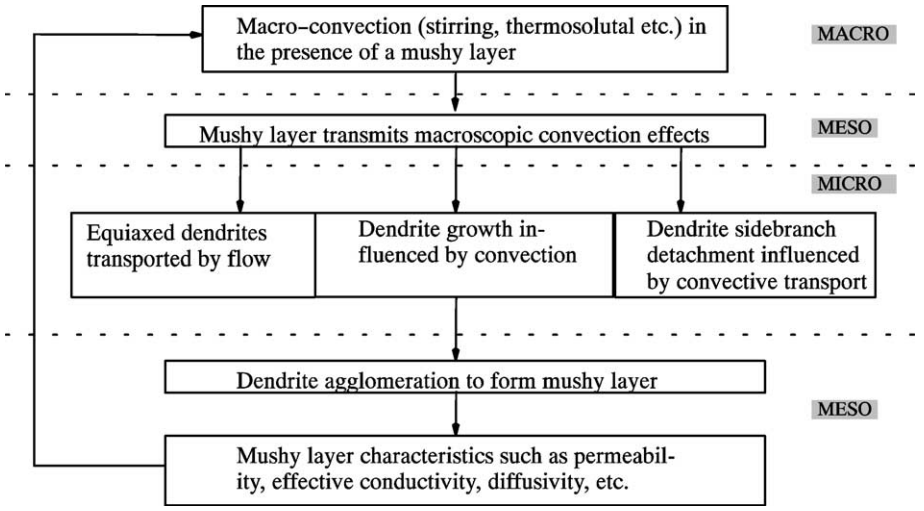

Fig. 3. The relationships between phenomena at the macro-, micro- and mesoscales pertaining to the transport and growth of dendrites in flow.

liquid and the variation of the solute concentrations in the interdendritic network. The numerical simulation of the mesoscale field will require modeling to obtain the envelope velocity $\overline{w}_{ne}$, the internal solid fraction f_i of the grain and the evolution of mesoscale properties (i.e. the average quantities $\langle\phi\rangle$) The models adopted for the mesoscale evolution will be a priori tested, i.e. they will be checked for physical realizability with the results of numerical simulations of the microscale. The subgrid scale model will then be provided by the evolution of the meso-level field. At the meso-level discrete particles representing the grains will be transported on the macro-grid and the averaging over this distribution will provide the properties of the mushy zone such as permeability, conductivity etc. If the number of particles in a grid cell is n and the average volume of the particles is $\overline{V}$ and the internal solid fraction of the grain is f_i, the solid fraction in the cell is $f_s = n\overline{V}f_i$. Thus the mixture quantities in the cell can be calculated. The value of n in a cell depends on the number of crystals in the cell which

includes the crystals nucleated in the cell and crystals transported to that cell in that time step. Subgrid modeling is required for obtaining $\overline{V}$ and f_i.

3. Interface resolution techniques

Very broadly, the methods for handling these problems can be classified into the so called *Eulerian*, *Lagrangian*, and the *Eulerian–Lagrangian* (Shyy et al., 1996). The *Lagrangian* method makes use of a moving grid in which a particular grid line is made to coincide with the interface. The required jump conditions are easily applied across the interface. Thus the interface is strictly treated as a discontinuity without any numerical diffusion. The Eulerian approach uses a fixed computational grid, and additional field variables are introduced to model the presence of a moving discontinuity on the computational grid. The interface is not explicitly tracked but has to be reconstructed from the distribution of certain field variable (Brackbill et al., 1992; Scardovelli and Zaleski, 1999; Voller and Prakash, 1987).

In the Eulerian–Lagrangian method a fixed computational grid is used along with explicit tracking of the interface by means of marker particles (Shyy et al., 1996, 1998). One can also resort to unstructured representation of the interface in three dimensions, with periodic remeshing. The interface is represented by a set of marker particles as a lower dimensional entity, i.e., a curve in a two-dimensional case and a surface in a three-dimensional case. The interface is advected according to the interfacial conditions like in the Lagrangian method.

3.1. Macroscopic simulation: moving grid method

The moving grid method can be fruitfully employed if the interface shape variations are not severe. For this reason, this approach is often used in the macroscopic model (Shyy, 1994). In our approach a combined Cartesian-contravariant velocity formulation is adopted. The Cartesian velocities serves as the primary variables, and the grid motion is handled through the definition of contravariant velocity components. Geometric conservation has been ensured through proper definition of metric terms for both convection and diffusion terms, and updating the jacobian in a consistent manner. For detailed information, see Shyy (1994).

For systems that can be cast under the Boussinesq approximation, the non-dimensional equations take the form:

$$\frac{\partial U_i}{\partial X_i} = 0$$

$$\frac{\partial U_i}{\partial \tau} + \frac{\partial U_j U_i}{\partial X_j} = -\frac{\partial P}{\partial X_i} + Pr\frac{\partial^2 U_i}{\partial X_i^2} - Ra\,Pr\,g_i$$

$$\frac{\partial \Theta}{\partial \tau} + \frac{\partial U_j \Theta}{\partial X_j} = \frac{\partial^2 \Theta}{\partial X_i^2}$$

The conduction heat transfer in the solid region is described by

$$\frac{\partial \Theta}{\partial \tau} = \frac{\partial^2 \Theta}{\partial X_i^2}$$

where, $Pr = v/\alpha$ is the Prandtl number, and Ra is the Rayleigh number. The Rayleigh number measures the strength of the buoyancy induced natural convection and is given by

$$Ra = \frac{g\beta_T(T_H - T_M)H^3 Pr}{v^2}$$

The Stefan condition, can be written in non-dimensional form as

$$V_N^* = St[(\nabla\Theta \cdot \vec{n})_s - (\nabla\Theta \cdot \vec{n})_l]$$

The Stefan number St is the ratio of sensible heat to the latent heat, $C_p(T_H - T_M)/L$, where C_p is the specific heat, T_H the temperature imposed on the melt pool, T_M the melting temperature, and L the latent heat.

We present an example with a moving solidification front in a rectangular domain (the aspect ratio between width and height = 2, depicted in Fig. 4. The left and right walls are of constant temperature, and the top/bottom walls are adiabatic. The parameters defining the problem thus are the Rayleigh number, Ra, the Prandtl number, Pr, the Stefan number, St; they are $Ra = 2.2 \times 10^5$, $Pr = 2.08 \times 10^{-2}$, and $St = 4.02 \times 10^{-2}$. In the moving grid technique, the grid needs to be regenerated at each time step because we require it to conform to the phase front which is constantly changing. Algebraic grid generation based on transfinite interpolation obtains the interior grid distribution in a domain from the distribution of points on the boundary of the domain. Stream function and temperature plots

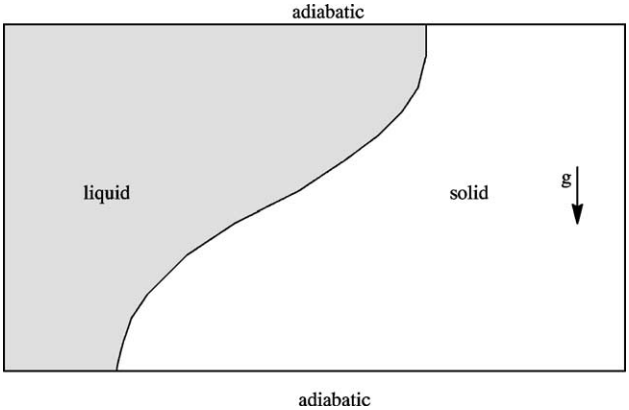

Fig. 4. Melting of a pure metal between vertical isothermal walls.

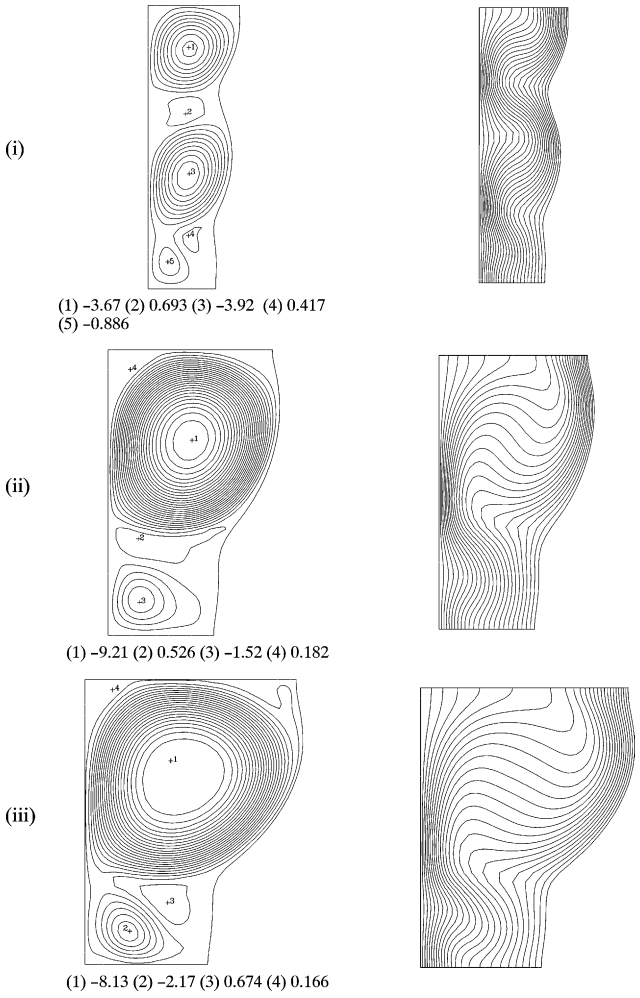

Fig. 5. Stream function and temperature contours in a solidifying melt contained in a rectangular domain, computed using the moving grid technique: τ (i) 0.83 (2 min) (ii) 2.07 (5 min) (iii) 2.76 (6.67 min).

are shown in Fig. 5. For more details, see Shyy et al. (1998).

In addition to employing the moving grid technique to model a phase boundary, one can also combine this approach with a fixed grid solidification model such as the enthalpy formulation (Shyy, 1994; Shyy et al., 1996; Voller and Prakash, 1987). In such a case, the moving grid technique performs the function of following the geometric variations of the rigid boundary, while the fixed grid solidification model handles the solidification dynamics without resorting to grid redistribution. Such an approach strikes a compromise between the various aspects of a very complicated process involving moving boundaries from both process operation (such as ampoule movement) and intrinsic physics (phase boundary movement). As an example, Bridgman growth of β-NiAl, an intermetallic, is discussed. In this case, the combination of the furnace enclosure and the ampoule presents a very complicated geometry. To render the computations tractable and simultaneously obtain adequate resolution in the ampoule region, a two-level strategy is employed. Level 1 simulates the entire domain and is referred to as the global furnace model. Level 2 concentrates on the ampoule region, with more refined mesh resolutions, and obtains its boundary conditions from the level 1 or the global simulation. With this two-level strategy, we can obtain useful information at the global level and yet obtain adequate resolution at the melt/crystal interface.

The computational technique in this case embodies the enthalpy formulation along with curvilinear meshing, consistent second-order discretization in strong conservation laws. The grid distribution is adjusted according to the movement of the ampoule. Stream function and isotherm distributions at two representative ampoule positions in this device are depicted in Fig. 6. Fig. 7 shows that the temperature distribution along

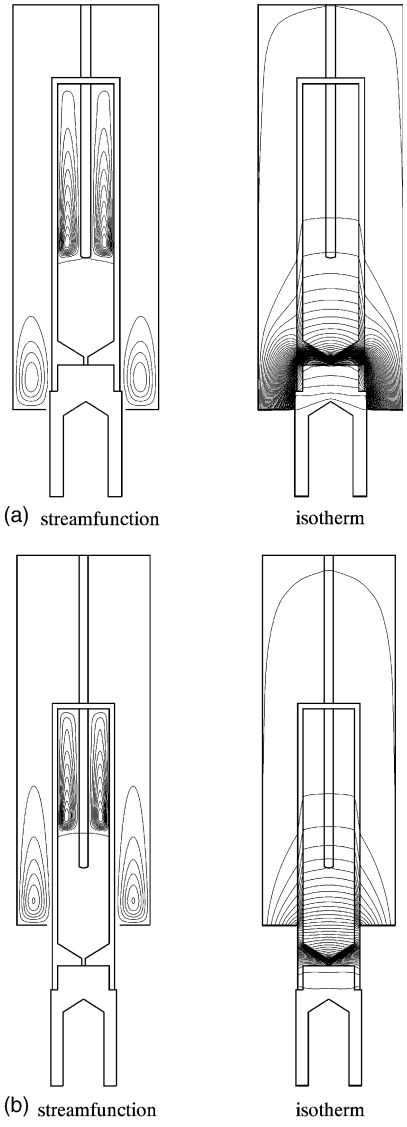

Fig. 6. Solution characteristics of NiAl solidification at two ampoule positions: (a) $H = 43$ mm and (b) $H = 87$ mm.

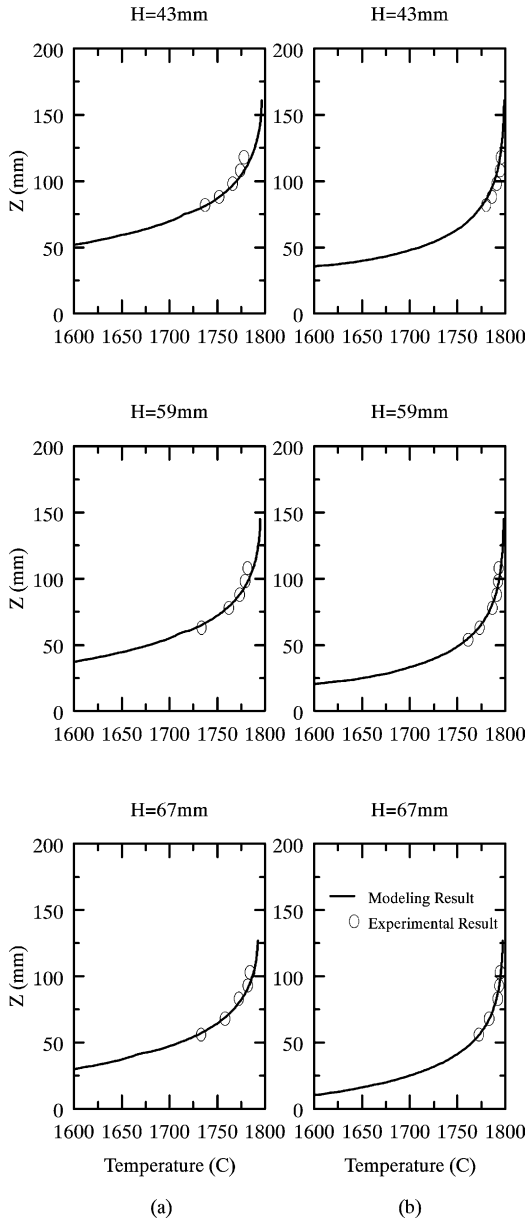

Fig. 7. Comparisons of temperature profiles along (a) the NiAl centerline, and (b) the ampoule outer wall between the modeling result and the experimental data for three ampoule positions.

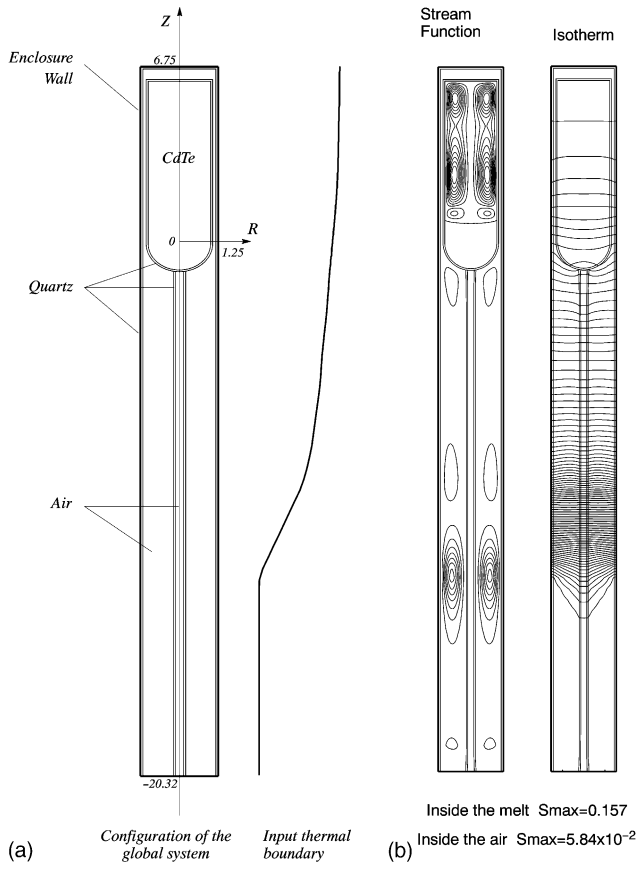

Fig. 8. The Bridgman growth system of CdTe: (a) the configuration and input thermal profile and (b) the stream function and isotherm distributions at $Ra = 10^5$.

the centerline and the ampoule outer wall obtained from the computational simulation matches the experimental measurements well.

Finally, we discuss the scale-up issue by presenting two simulations of identical geometrical shapes and thermal boundary conditions, but with different physical dimensions. Fig. 8(a) depicts a Bridgman system for growing the CdTe crystal, with the input thermal profile shown. These II–VI materials combine elements with two and six valence electrons, and are attractive for future development in telecommunication and wireless computing. Scale-up of the chip size during solidification is highly desirable. However, the convection–conduction effects often cause compositional variations in such materials, and better knowledge is needed to guide improved processing techniques. To demonstrate the issues, we first consider a small, laboratory scale, the Rayleigh number based on the ampoule radius is 10^5. Fig. 8(b) shows the stream function and isotherm distributions. If we scale up the dimension of the system by a factor of 10, then the Rayleigh number becomes 10^8, a thousand times increase. Consequently, the thermal environment within both ampoule and furnace becomes intrinsically unsteady, due to the much larger buoyancy effect. The stream function and isotherm distributions at selected time instants for this case are shown in Fig. 9. Clearly, the flow field experience much fluctuation in time, which results in thermal and compositional inhomogeneity. An important implication is that the solid-melt interface will experience time dependency in shape and in location, which, as mentioned, can substantially affect the quality of the crystal. The computational tool can play a critical role in helping extrapolate our knowledge in the scale-up process.

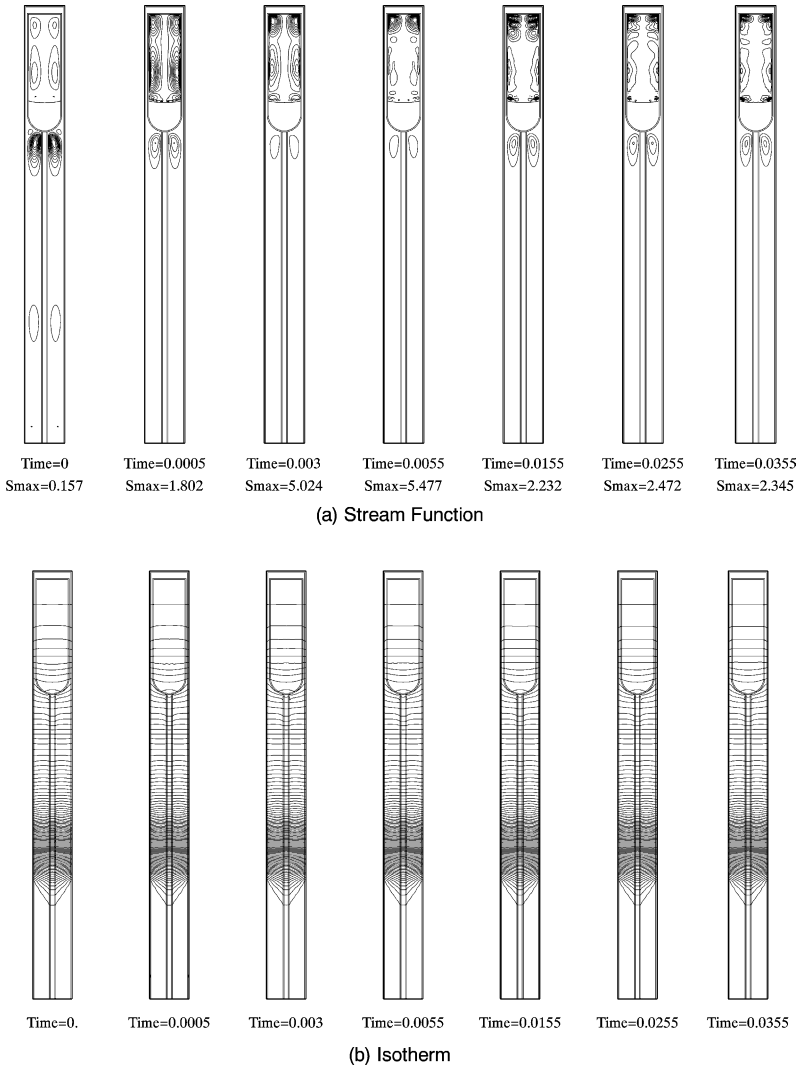

Fig. 9. The stream function and isotherm distributions of the Bridgman growth of CdTe at $Ra = 10^8$. Compared to the case shown in Fig. 8, the present system is 10 times bigger in dimension, and is intrinsically unsteady due to stronger buoyancy.

3.2. Morphological simulation: fixed grid method

For the micro-level simulations where the information such as curvature is needed in order to incorporate the capillary effects, it is often desirable to explicitly track solid–liquid boundaries without smearing the interface. We have developed a numerical technique for tracking unstable solidification fronts, in which the interface is tracked over a fixed Cartesian grid by means of marker particles (Shyy et al., 1996; Udaykumar et al., 1999). Thus, the interface is maintained as a discontinuity. Accurate interfacial properties such as normals and curvatures can be extracted. The development of microstructures of considerable complexity can be tracked using the technique. In this approach, the interface is tracked as a discontinuity and boundary conditions of the Dirichlet/Neumann type are applied on the tracked fronts. The discretization to include the embedded boundaries involves simple measures in the vicinity of the interface. However, one should also note that instead of a deterministic model, one can adopt a stochastic approach to track the evolution of the microstructures (Nastac, 1999, 2000). We will not discuss this approach here. In our approach, for the solidification problem the interface velocity is computed directly from the Stefan condition, and the normal gradients of the temperature are evaluated to second-order accuracy. The curvature dependent boundary conditions are imposed at the exact interface location. The problem of stiffness of the interface evolution in curvature-driven growth is surmounted by using an implicit formulation to couple the interface evolution with temperature field evolution. The issue of change of phase of a grid point when the boundary crosses over it is dealt with by a simple analogy with purely Lagrangian methods. This involves redefinition of the stencils in the points

adjoining the interface to account for the grid points that have changed phase. The various components of the solution algorithm can easily be extended to 3D. To illustrate the performance of this method, we consider a crystal solidified in a pure undercooled melt. The diffusion equation takes the form

$$\frac{\partial \phi}{\partial t} = \nabla \cdot \alpha_i \nabla \phi$$

where α_i is the diffusion coefficient of phase i. The interface is then at a temperature $\phi = 0$ and the front velocity is given by

$$V_n^* = St\left(\frac{k_s}{k_L}\left(\frac{\partial \phi}{\partial n}\right)_s - \left(\frac{\partial \phi}{\partial n}\right)_l\right)$$

In each of the calculations below we place a seed crystal in a domain with insulated boundaries. The initial condition is a uniformly undercooled melt with the conditions

$T(\vec{x}, 0) = St$ in the liquid

$T(\vec{x}, 0) = 0$ it in the solid

Note that the initial condition applied here corresponds to a nucleus of solid placed instantaneously in an undercooled melt. The boundary conditions at the interface for the temperature includes the effect of capillarity and attachment kinetics and is given, in non-dimensional form by a generalized Gibbs–Thomson condition

$$T_i + \left(\frac{c_l}{c_s} - 1\right)T_i^2 + \sigma(\theta)\kappa + \mu(\theta)V_i = 0$$

For the surface energy parameter σ and attachment kinetics parameter μ, the following forms are adopted

$$\sigma(\theta) = \sigma\left(1 + A_s\left[\frac{8}{3}\sin^4\left(\frac{1}{2}m(\theta - \theta_0)\right) - 1\right]\right)$$

$$\mu(\theta) = \mu\left(1 + A_k\left[\frac{8}{3}\sin^4\left(\frac{1}{2}m(\theta - \theta_0)\right) - 1\right]\right)$$

The above expressions model the anisotropic natures of the solid–liquid interface energy and kinetics. These parameters can result in the morphological characteristics along certain crystallographic directions (Howe, 1997). The role of surface energy is intrinsic in considering solidification dynamics at the morphological scale. Furthermore, if the solidification rate is fast and the thermodynamic non-equilibrium is present, then the kinetic process needs to be modeled. Here, we have adopted simple expressions to highlight the influences of the surface energy and kinetics parameters. A sixfold symmetry is assigned (Udaykumar et al., 1999) in the examples presented below, namely, $m = 6$, to examine the effects of anisotropy on the growth of interfaces. Based on our approach, the field calculation is second-order accurate while the position of the phase front is calculated to first-order accuracy. Furthermore, the accuracy estimates hold for the cases where there are property jumps across the interface. In Fig. 10 we compute the growth of an initially fourfold-symmetric seed crystal in an undercooled melt with a sixfold-symmetric surface energy. The parameters used for the case in Fig. 10(a) are of higher surface energy coefficient and kinetic rate constant than that in (b). Both calculations were performed on a 500×500 grid. The effect of the sixfold anisotropy is to promote growth in the preferred directions to yield a sixfold symmetric structure. The finer scales displayed by the more unstable lower surface energy case is consistent with the expected physics. Recently, Zhao and Heinrich (2001) have employed front-tracking finite element method to simulate the same morphological instability problems.

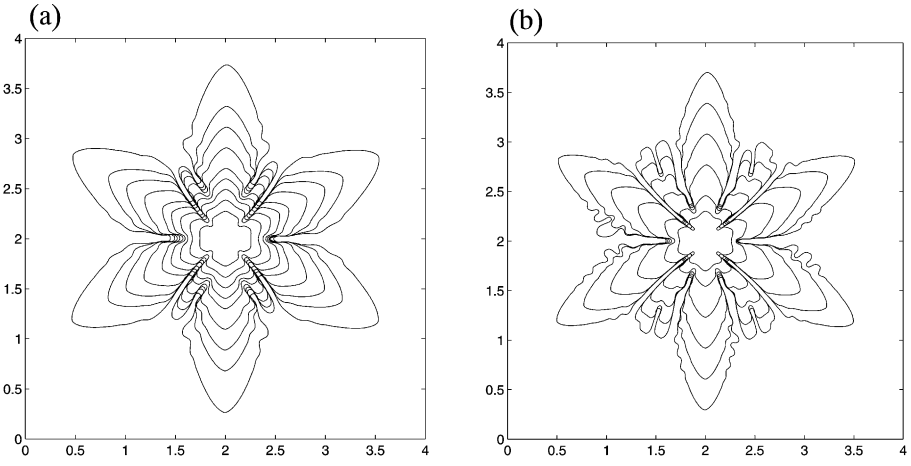

Fig. 10. Sixfold symmetric anisotropy in surface energy, simulations using a 500×500 grid, $St = 0.8$. (a) Higher surface energy and kinetic rate case: surface energy parameter $\sigma = 0.002$, surface energy kinetics parameter $\mu = 0.002$, surface energy anisotropy $A_s = 0.4$, kinetics anisotropy $A_k = 0$. (b) Lower surface energy and kinetic rate case: surface energy parameter $\sigma = 0.001$, kinetic parameter $\mu = 0.001$, surface energy anisotropy $A_s = 0.4$, kinetics anisotropy $A_k = 0$.

4. Concluding remarks

Substantial effort has been made in computational modeling and simulation for crystals and alloys solidification processing. One of the major trademarks of this area is that it is truly interdisciplinary expertise from many areas including materials science and engineering, fluid dynamics, heat and mass transfer, numerical analysis, scientific computing and visualization, and process design is required. Many challenges remain. For example, issues of accurate estimation of the geometric information, such as curvature, have not been satisfactorily resolved. Progress has been made in this direction based on the existing foundation in geometric modeling (Jayaraman et al., 1997). In particular, in the context of large scale fluid flow and solidification phenomena, both fixed and moving grid techniques can be utilized (Shyy, 1994; Shyy et al., 1996, 1998; Udaykumar et al., 1999; Zhao and Heinrich, 2001). For morphological levels of simulation, a fixed grid approach may be more suitable. Nevertheless, to our knowledge, in the context of a sharp interface computation, no robust and accurate algorithm (i.e., with accuracy comparable to a second-order field equation solver) has been reported, via numerical demonstration, for three-dimensional surface representation with moving boundaries. Multi-scale modeling from morphological to global scales is progressing; however, numerical and modeling uncertainties need to be further clarified. One should also emphasize that systematic experimental information, with satisfactory accuracy while encompassing the length scale range discussed in this article, is largely lacking. Without parallel efforts between computation, modeling, and experimentation, it will be difficult to advance our knowledge and predictive capability in a systematic and comprehensive manner. It is anticipated that progress will be realized if concerted efforts are made in all these relevant areas.

Acknowledgements

The work presented was partially sponsored by AFOSR and Pratt & Whitney. The research was conducted in collaboration with Drs. H. Ouyang and H.S. Udaykumar and Mr. S. Pal.

References

Beckermann, C., Viskanta, R., 1993. Mathematical modeling of transport phenomena during alloy solidification. Appl. Mech. Rev. 46, 1–27.

Brackbill, J.U., Kothe, D.B., Zemach, C., 1992. A continuum method for modeling surface tension. J. Comp Phys. 100, 335–354.

Flemings, M.C., 1974. Solidification Processing. McGraw-Hill, New York.

Ganesan, S., Poirier, D.R., 1990. Conservation of mass and momentum for the flow of interdendritic liquid during solidification. Metall. Trans. B 21B, 173–181.

Howe, J.M., 1997. Interfaces in Materials. Wiley, New York.

Hurle, D.T.J. (Ed.), 1993. Handbook of Crystal Growth, Vol. 1: Fundamentals. North-Holland, Amsterdam, The Netherlands.

Jayaraman, V., Udaykumar, H.S., Shyy, W., 1997. Adaptive unstructured grid for three-dimensional interface representation. Numer. Heat Transfer, Part B 32, 247–265.

Nastac, L., 1999. Numerical modeling of solidification morphologies and segregation patterns in cast dendritic alloys. Acta. Mater. 47, 4253–4262.

Nastac, L., 2000. A stochastic approach for simulation of solidification morphologies and segregation patterns in cast alloys. MCWASP IX (SIM2000), Aachen, Germany.

Scardovelli, R., Zaleski, S., 1999. Direct numerical simulation of free-surface and interfacial flow. Ann. Rev. Fluid Mech. 31, 567–603.

Shyy, W., 1994. Computational Modelling for Fluid Flow and Interfacial Transport. Elsevier, Amsterdam, The Netherlands.

Shyy, W., Thakur, S.S., Ouyang, H., Liu, J., Blosch, E., 1997. Computational Techniques for Complex Transport Phenomena. Cambridge University Press, UK.

Shyy, W., Udaykumar, H.S., 2000. Multiscale modeling for solidification processing. In: Sunden, B., Comini, G. (Eds.), Computational Analysis of Convection Heat Transfer. WIT Press, Southampton, UK, pp. 141–198.

Shyy, W., Pal, S., Udaykumar, H.S., Choi, D., 1998. Structured moving grid and geometric conservation laws for fluid flow computation. Numer. Heat Transfer, Part A 34, 369–397.

Shyy, W., Udaykumar, H.S., Rao, M.M., Smith, R.W., 1996. Computational Fluid Dynamics with Moving Boundaries. Hemisphere, Washington, DC.

Udaykumar, H.S., Mittal, R., Shyy, W., 1999. Computation of solid–liquid phase fronts in the sharp interface limit on fixed grids. J. Comput. Phys. 153, 535–574.

Voller, V.R., Prakash, C., 1987. A fixed grid numerical modeling methodology for convection–diffusion mushy region phase-change problems. Int. J. Heat Mass Transfer 30, 1709–1719.

Wang, C.Y., Beckermann, C., 1994. Prediction of columnar to equiaxed transition during diffusion-controlled dendritic alloy solidification. Metall. Mater. Trans. 25A, 1081–1093.

Wang, C.Y., Beckermann, C., 1996. Equiaxed dendritic solidification with convection: Parts 1–3. Metall. Mater. Trans. 27A, 2754–2795.

Worster, M.G., 1997. Convection in mushy layers. Ann. Rev. Fluid Mech. 29, 91–122.

Zhao, P., Heinrich, J.C., 2001. Front-tracking finite element method for dendritic solidification. J. Comp. Phys. 173, 765–796.